Multi-Objective Optimization of Modular Multilevel Converter Systems

Nikolaus Patzelt, Christian Schlegel, Michail Vasiladiotis
Hitachi Energy
Spinnereistrasse 3
5300 Turgi, Switzerland
Email: nikolaus.patzelt@hitachienergy.com, christian.schlegel@hitachienergy.com,
michail.vasiladiotis@hitachienergy.com

Keywords

≪Modular Multilevel Converters (MMC)≫, ≪Multi-Objective Optimization≫, ≪Optimization Method≫, ≪Railway Power Supply≫.

Abstract

This paper investigates a multi-objective optimization method for modular multilevel converter systems. The method is applied to the AC-AC MMC topology, which connects the three-phase utility grid to the single-phase railway grid. The presented paper aims at a joint optimization of all system components providing a set of pareto-optimal system designs. The optimization space encompasses core system design parameters, such as the number of cells in a branch, the sizing of cell capacitor and branch inductance, but also the switching frequency and other parameters. The objectives studied in this paper are the overall system cost and losses. The considered constraints comprise limitations on system components as well as the power capability of the converter, compliance with grid codes and system efficiency. The obtained optimized design improved the total system cost by 7 % compared to a manually derived benchmark design. It has been verified by offline and real-time simulations.

Introduction

The considered AC-AC static frequency converter is based on the modular multilevel converter topology [1][2]. An integrated gate-commutated thyristor (IGCT)-based MMC for railway power supply is introduced in [3] and [4]. It connects the three-phase 50 Hz utility grid to a single-phase 16.7 Hz railway supply and consists of an arbitrary number of cells N connected in series along one branch and a branch inductor as shown in Fig. 1. The branch is the sub-circuit connecting a three-phase line with the single-phase line. Every bipolar cell consists of a full-bridge circuit, a capacitor, a clamp circuit and a bypass thyristor. The entire system includes the converter as well as the equipment interfacing to the utility and railway grid such as transformers and possibly filters.

In state-of-the-art converter designs, typically, a set of individually optimized components are derived. The combination of these components then serves as a design candidate. However, as the converter system is highly non-linear, an analytical system optimization is challenging and the trade-off between the different design parameters is not obvious. This paper proposes a method to jointly optimize various design parameters for different objectives simultaneously to achieve an improved overall system design.

In the past years, there have been other approaches trying to optimize MMC system design. In [5], an optimization with parameter variation is suggested, based on which the passive components are dimensioned. In [6], a minimization of the capacitor sizing is achieved by optimizing the arm circulating current as well as the common mode voltage, leading to decreased energy storage requirements of the MMC. A multi-objective optimization for the converter design has been performed in [7] and [8]. These studies focus on footprint rather than cost of the converter and consider the design of the converter itself.

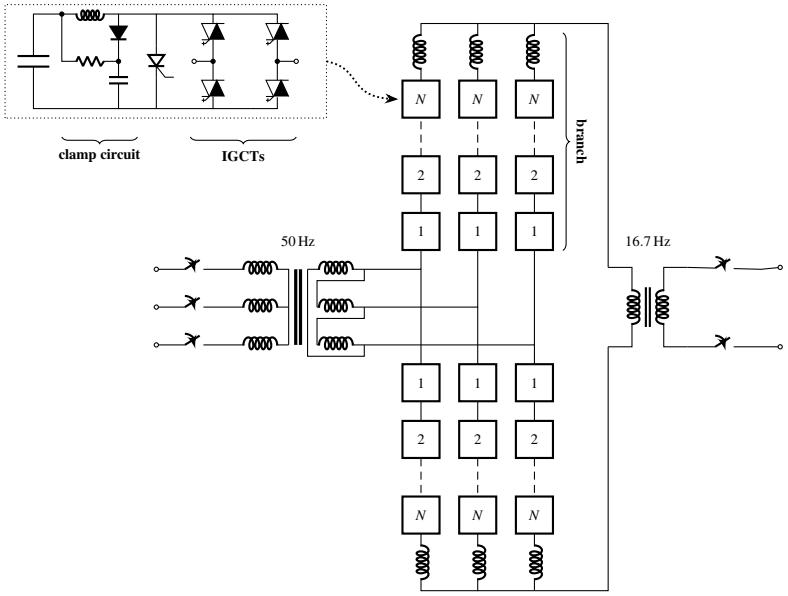

Fig. 1: AC-AC Modular Multilevel Converter for Railway Interties.

In contrast, this paper focuses on the steady-state and dynamic behaviour of the converter system including grid interface components such as transformers and filters. Moreover, the interaction with the system environment is studied considering different grid impedances and operating points.

To perform an optimization it is necessary to define an objective function vector with objectives as well as a set of constraints. The multi-objective optimization problem formulation is shown in (1) [9].

$$\begin{aligned} \min \quad & \mathbf{f}(\mathbf{x}) \\ \text{subj. to} \quad & g_j(\mathbf{x}) \leq 0 \quad \forall j \in [1,m] \\ & h_k = 0 \quad \forall k \in [1,p] \end{aligned} \tag{1}$$

The objective function is given by $\mathbf{f} : V \rightarrow \mathbb{R}^n$ with $\mathbf{f}(\mathbf{x}) = (f_1(\mathbf{x}), f_2(\mathbf{x}), \ldots, f_n(\mathbf{x}))$.

Here n is the number of different objectives for a given optimization problem. The domain V with $\mathbf{x} \in V$ represents the set of design parameters, which, in the presented application, is a finite and closed set.

Structure of the System Design Optimization

The optimization method consists of four parts: (a) The parameter input, (b) the design derivation, (c) the design evaluation and (d) the optimization. The schematic of the optimization approach is shown in Fig. 2. The algorithm is based on a defined set of variable design parameters, which shall be optimized.

During each iteration step i, a set $\mathcal{S}_i$ of design parameters is chosen (a). During the design derivation (b), a design d_i is determined in two steps. Step 1 defines internal design parameters and derives the converter parameters. Step 2 calculates the system behavior in the frequency domain considering the system environment, such as grid impedances. The resulting design is checked for constraint violations.

As a next step, the suggested designs must be evaluated (c). Here, cost functions are used for evaluation, assigning a cost vector to the design d_i. In Fig. 2 the material cost and the losses are shown as an example. However, any design objective can be used here. Finally, the design is assessed according to the objectives in comparison to the previously analyzed designs (d). Depending on the optimization algorithm, a new set of parameters $\mathcal{S}_{i+1}$ is generated in order to evaluate the newly calculated design d_{i+1}.

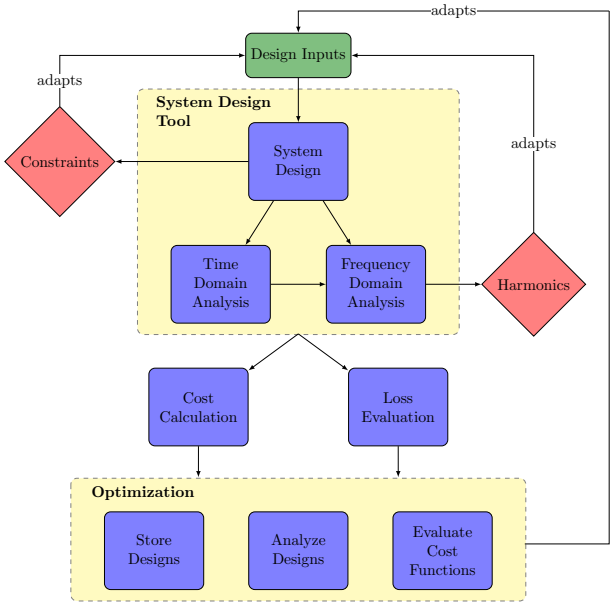

Fig. 2: Schematic Description of Proposed Multi-Objective Optimization Method.

Convergence

In order to ensure feasibility of the optimization, the convergence of the multi-objective optimization has been studied for the AC-AC MMC topology. Convergence is defined according to the stopping criterion given in [10] and a generation shall consist of 120 designs. Particularly relevant are the number of design parameters and the number of objectives. Fig. 3a shows several performed optimizations, relating the number of design parameters to the iterations until convergence. The number of parameters influences the convergence. In red the linear regression is shown to underline the trend.

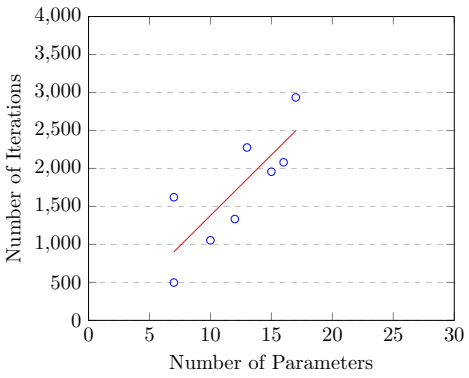

(a) Number of iterations until full convergence of multi-objective optimization.

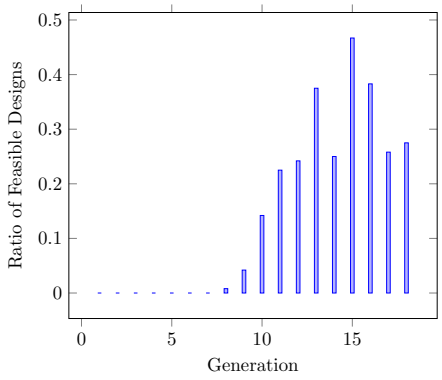

(b) Discovery of feasible designs, given by the ratio of feasible to all evaluated designs.

Fig. 3: Convergence of the Multi-Objective Optimization.

The ratio of discovered feasible designs versus unfeasible designs shifts towards feasible designs in the course of the optimization as shown in Fig. 3b. Particularly in the first generations few feasible designs are being found, while after nine to ten generations, feasible designs are being discovered constantly.

Optimization Problem

Objective Function

This paper suggests a multi-objective optimization focusing on material cost and system losses. To quantify the material cost, individual cost functions for all parts of the converter system have been derived.

The sum of these costs defines the first objective. The components considered are

- MMC cells including base frame
- Branch inductances
- Single- and three-phase transformer
- Single- and three-phase filter
- Cooling unit.

The second objective are the system losses. They are the main contributor to the life cycle cost of a converter system and a key parameter defining the performance of a design. The system losses are calculated according to (2).

$$f_2(\mathbf{x}) = \mathbf{w}^\top \cdot \mathbf{L} \tag{2}$$

Here, $\mathbf{L}$ represents losses for different operating points weighted according to a pre-defined weighting function $\mathbf{w}$. The considered losses represent the system losses instead of the converter losses alone. Thus, the losses in the filters, transformers and cooling units are considered as well.

Constraints

The optimization objectives, constraints and design parameters need to be chosen carefully. To obtain a feasible solution, the mathematical formulation must contain all constraints that are attached to the optimization problem. Some constraints are inherent to the design. Other constraints are imposed by the system environment. The constraints that have been considered are shown in Table I. They encompass constraints on the components such as branch inductance, cell capacitance and the number of cells, power capabilities, the compliance with grid codes considering different frequency-dependent grid impedances as well as the system efficiency.

Table I: List of Constraints.

Description	Variable	Constraint
Branch inductance	L_{br}	$L_{\text{br,min}} < L_{\text{br}}$
Cell capacitance	C_{cell}	$C_{\text{cell,min}} < C_{\text{cell}} < C_{\text{cell,max}}$
Number of cells	N	$N_{\text{min}} < N$
Set of power ref. points (3-ph)	$\vec{S}_{\text{3ph}}$	$\vec{S}_{\text{3ph,req}} < \vec{S}_{\text{3ph}}$, diff. V levels
Set of power ref. points (1-ph)	$\vec{S}_{\text{1ph}}$	$\vec{S}_{\text{1ph,req}} < \vec{S}_{\text{1ph}}$, diff. V levels
V THD (3-ph, 1-ph)	THD_{V}	$THD_{\text{V}} < THD_{\text{V,max}}$
I THD (3-ph, 1-ph)	THD_{I}	$THD_{\text{I}} < THD_{\text{I,max}}$
V harm. content (3-ph, 1-ph)	$\vec{V}_{\text{harm}}$	$\vec{V}_{\text{harm}} < \vec{V}_{\text{harm}}^{\text{max}}$
I harm. content (3-ph, 1-ph)	$\vec{I}_{\text{harm}}$	$\vec{I}_{\text{harm}} < \vec{I}_{\text{harm}}^{\text{max}}$
Total system efficiency	η	$\eta_{\text{req}} < \eta$

Design Parameters

There is a high number of design parameters which can be taken into account when designing the converter system. However, while some may have a large impact, others only affect the objectives marginally. The most important design parameters are introduced in the following:

- **Switching frequency**: The switching frequency is selected based on the modulation technique and depending on the project specification. While higher switching frequencies reduce the harmonic content produced in the system, they increase the losses through switching.
- **Cell utilization**: The chosen number of cells could differ from the calculated value for the minimum required number of cells. Thus, the actual power capability of the converter may exceed the minimum required power capability. This power margin can be used to reduce either the current in the branch or the average cell voltage. The cell utilization defines whether the current or the voltage is minimized and has been used as a design parameter in the optimization.

- **Cell capacitor ripple**: The cell capacitor ripple (Δv_{cell}) directly influences the sizing of the capacitor itself. If a higher capacitor voltage ripple is allowed, the capacitor can be sized smaller. The cell capacitance is calculated by

$$C_{\text{cell}} = 2 \cdot \frac{\Delta E_{\text{br}}^{\max}}{N((V_{\text{cell}}^{\min} - V_{\text{cell}}^{\max})^2)} \tag{3}$$

  where $\Delta E_{\text{br}}^{\max}$ is the maximum energy variation in the branch. Due to the dependence on the maximum ($V_{\text{cell}}^{\max}$) and minimum cell voltage ($V_{\text{cell}}^{\min}$), the cell capacitance can be steered by defining the cell capacitor ripple.
- **Transformer impedance**: A transformer impedance (X_{trafo}) is present in the design for the grid transformers on the single- and three-phase side as shown in Fig. 1.
- **Number of cells**: The number of cells per MMC branch (N).
- **Filter type**: On single- and three-phase side different filter types are evaluated.
- **Filter power**: The filter power determines the dimensioning of the individual filter components depending on the filter type.

Optimization Results

With the multi-objective optimization procedure, it is possible to analyze the relevance of different design parameters with respect to the selected objectives. This enables the designer to reduce the set of parameters to the most influential ones. To identify these, an analysis of the respective variable relevance has been performed. The correlation of different design parameters with the defined objectives and constraints has been assessed with the Pearson correlation coefficient $\rho_{\text{X,Y}}$, relating the random variables X and Y with

$$\rho_{\text{X,Y}} = \frac{1}{\sigma_x \sigma_y} Cov(X,Y), \tag{4}$$

where $Cov(X,Y) = \mathbb{E}[(X - \mathbb{E}[X]) \cdot (Y - \mathbb{E}[Y])]$ and σ_x and σ_y are the standard deviation of X and Y, respectively. Random variable X represents a design parameter, where Y represents an objective or constraint. The correlation can take values in the interval $[-1,1]$, where a Pearson correlation of -1 indicates fully negative linear correlation and a value of 1 indicating total positive correlation. If the value is in the area around 0, there is no correlation detected. While this correlation gives good results for linear correlations, it may fail to detect other types of correlations. Fig. 4 illustrates the impact of five different design parameters on the cost, the losses, and the harmonics of the converter system.

Fig. 4a shows that the main driver of the material cost is the number of cells. This correlates with the intuition that the most cost-efficient design is a design with a minimum number of cells. There are, however, also other parameters that influence the cost. Most notably, this is the cell capacitor voltage ripple. The lower Δv_{cell} becomes, the lower is the required number of cells in the branch. The losses are mainly influenced by the switching frequency (Fig. 4b). This follows the argument of dependence of the switching losses to the switching frequency with $P_{loss,sw} \propto f_{sw}$. There are also many other factors influencing the loss calculation. This makes it hard to evaluate, which parameters are the most relevant. However, it can be said that due to the complexity and non-linearity of the topology, many parameters should be regarded when it comes to the loss evaluation of the system. It should be noted that the influence of the number of cells on the losses is only of an indirect nature. Increasing the number of cells allows to decrease the switching frequency and either cell voltage or branch current, leading to lower losses. Increasing the admissible cell capacitor ripple generally decreases the losses. While it is hard to take all the non-linear effects into account, this can be rooted in the positive correlation of the cell ripple with the number of cells. As the number of cells increases, the switching frequency can be decreased leading to lower losses. The harmonics are influenced by the respective transformer impedance. Moreover, the number of cells and again the switching frequency influence the harmonics.

These results are based on the analysis of various designs and their performance in terms of fulfillment of objectives or constraint violations. Another example of variable correlation is shown in Fig. 5. It

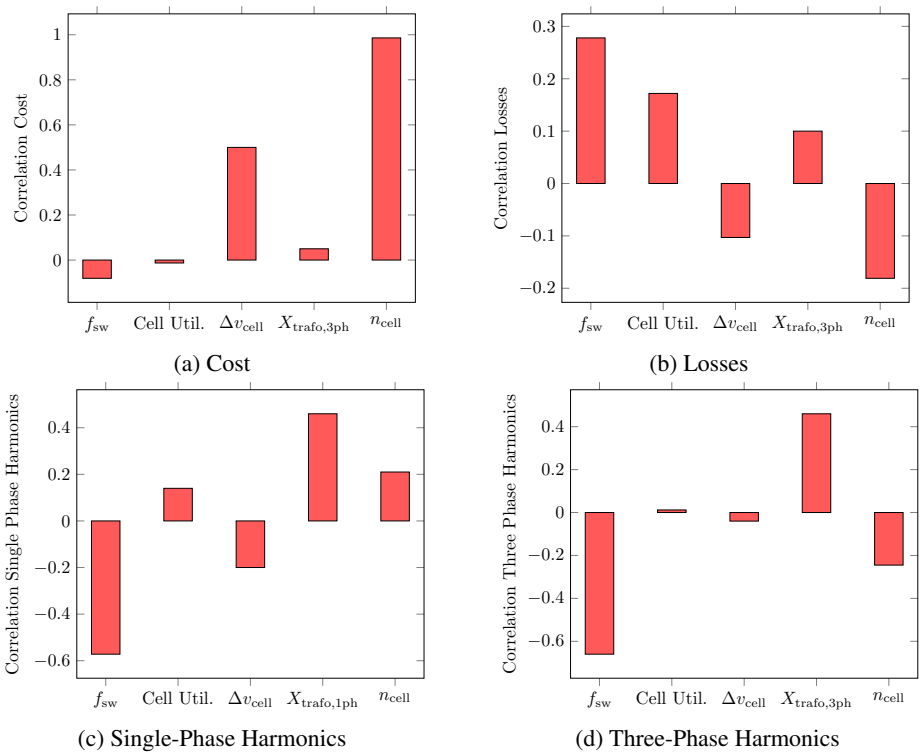

Fig. 4: Influence of various converter variables.

gives an example of a correlation between cell capacitor ripple and the required number of cells. There is a clear linear trend between capacitor ripple and the required number of cells. This also impacts the actual number of required cells and, thus, influences costs and losses of the design. Using such input-to-objective correlations, the design parameters can be analyzed and reduced to the most significant ones.

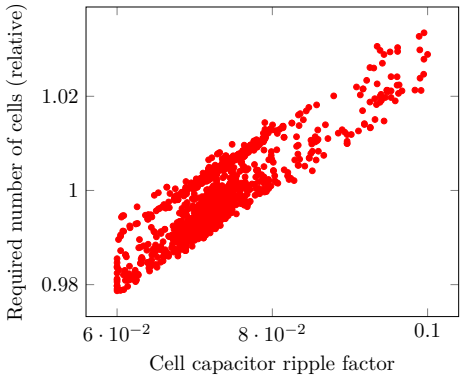

Fig. 5: Correlation between cell capacitor voltage ripple and the number of cells with the minimum number of cells N_{calc} as a function of the cell capacitor voltage ripple factor.

The optimization evaluates the design space, considering the introduced constraints optimizing for the objectives of total system cost and losses. The results of the optimization are compared with a benchmark design, which has been manually derived and which is verified and tested. The pareto-front of optimal designs is shown in Fig. 6. The proposed design, which has been derived from the optimization, is indicated as blue circle, and the existing manually derived benchmark design is shown as a blue rectangle. Two main clusters can be found that show a considerable cost difference. This is mainly due to the different number of cells, which is also considered in the design space of the optimization. As such, the optimization method can find improved designs reducing the required number of cells per branch.

During the verification of the dynamic behavior of designs, i.e. offline computer simulations, further

constraints are introduced to the objective space. In the steady-state analysis of the converter system these are not considered yet as this would lead to an unacceptable run-time of the optimization. Therefore, in Fig. 6 pareto-optimal designs exist which become unfeasible in the verification step. This is not yet considered in the automated optimization shown in Fig. 2. As such, the currently proposed design appears to be sub-optimal in Fig. 6.

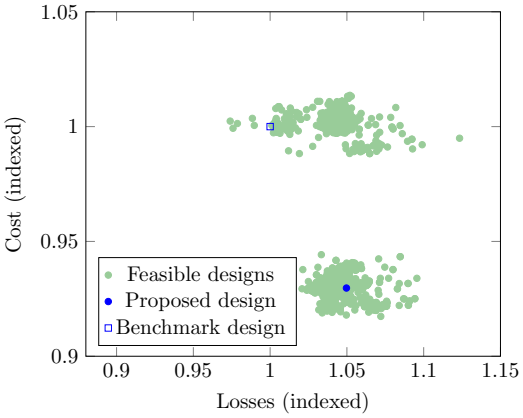

Fig. 6: Trade-off between cost and losses. Two clusters of evaluated designs are visible (green) with the benchmark design (blue square) in the cluster with higher system cost and the proposed design (blue circle) in the lower-cost cluster. Cost and losses are normalized based on the benchmark design.

Design Verification

In order to verify the obtained designs, different simulations are executed considering the full closed-loop control performance of the converter system. In a first step, offline computer simulations are conducted to verify that the dynamic behavior of the design does not violate any constraints. In a second step real-time simulations (RTS) with hardware-in-the-loop (HIL) are performed on different transient scenarios to confirm that the chosen designs fulfill the defined system requirements.

Offline Computer Simulations

Current Reference Step

The response of the converter to a current reference step on the three-phase side can be seen in Fig. 7. A reference step from 0.1 p.u. to -0.4 p.u. is performed. The reference is followed by a quick transient and without oscillations after the step. The closed-loop control performance of the suggested system design is comparable to the one of the benchmark design.

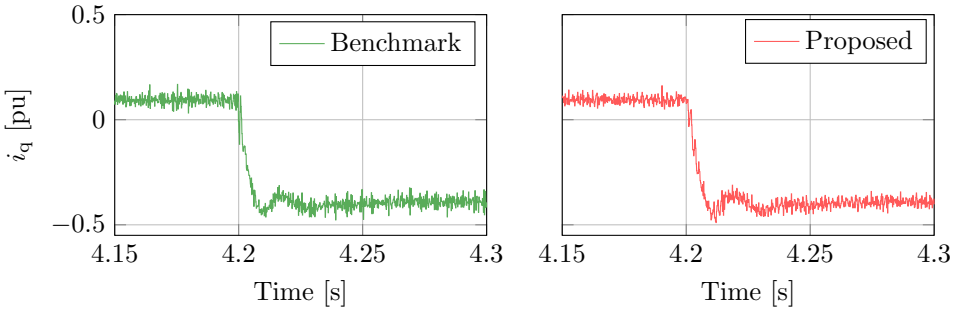

Fig. 7: Behavior of i_q after a reference current step. Comparison of offline computer simulations for the benchmark and the proposed design.

Three-Phase Grid Fault

A critical test for the performance of a system design is a grid fault scenario. A short-circuit is simulated and the resulting behavior is analyzed. In Fig. 8 the dynamic response in case of a fault on the three-phase

utility grid side is shown. Visible is the behavior of the three-phase grid side voltages and currents. The benchmark design is shown in green while the proposed optimized design is shown in red. For the same trajectory of the primary grid voltage $u_G(t)$ it is visible that the transient behavior of the grid current $i_G(t)$ is comparable, both during the fault as well as after voltage recovery. Thus, the results confirm the appropriate behavior of the suggested design during a three-phase grid fault.

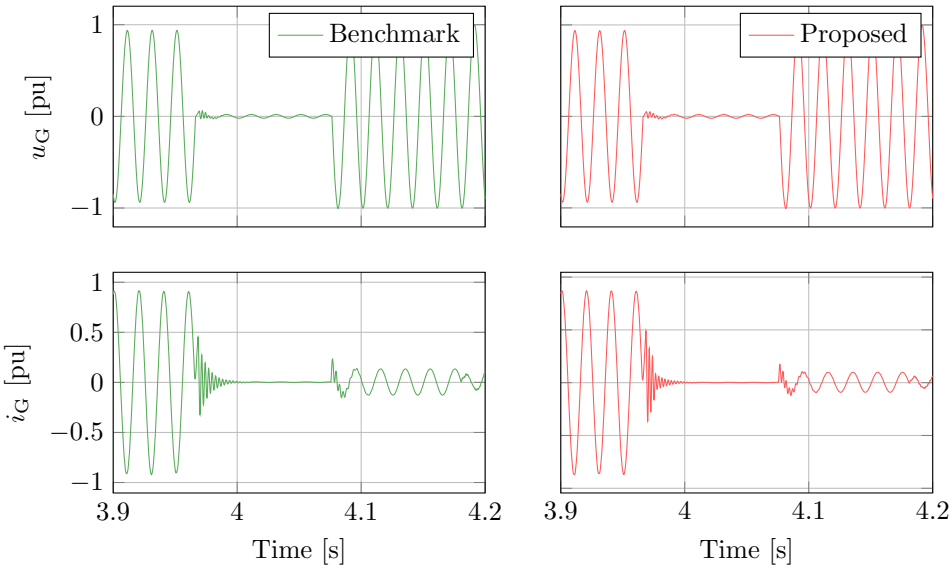

Fig. 8: Three-phase grid voltages and currents during a grid fault in offline computer simulations.

Real-Time Simulations

In a second step, real-time simulations are conducted. In this case, the real-time software and firmware are running on the actual control hardware, while the power system including MMC, transformers, filters and the AC grids is emulated in a commercial HIL system. To verify the design, various scenarios have been simulated. They include a current reference step, a grid fault, a power reference step, and a load step. The results are compared with the benchmark design.

Current Reference Step

In Fig. 9 the real-time simulation results of a current reference step are shown. The behavior is comparable both in the transient behavior as well as the recovery after the step. It is noted that the step change is different between the two designs (-0.4 p.u. for the benchmark and -0.5 p.u. for the proposed design, respectively) without loss of generality. Both designs show an acceptable and comparable current trajectory.

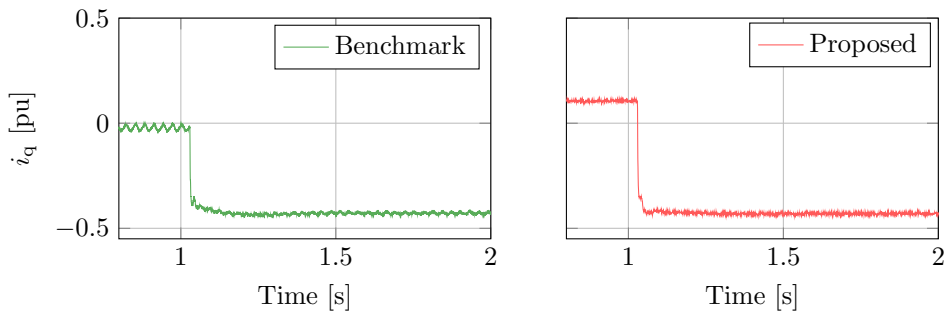

Fig. 9: HIL simulations of i_q after a reference current step for the benchmark and the proposed design.

Three-Phase Grid Fault

The real-time simulation of a fault in the utility grid is shown in Fig. 10. The upper plot shows the grid voltages for the benchmark and proposed design, respectively. The left plots show the occurrence of

the fault while the right plots show the voltage return. The voltage behavior matches between the two designs.

The lower plots show the grid currents. Here, a different behavior is observed. In the proposed design, after return of the voltage an inrush-current is visible. The latter occurs due to saturation in the transformer. The differently designed transformer in the benchmark design does not saturate and, thus, leads to lower inrush-currents. On the other side, the benchmark design has to bear higher filter currents as the filter gets excited. The proposed design is robust enough to meet the design requirements taking into account the non-linear behaviors of the system. The different designs lead to different dynamic behavior during a grid fault, with both behaviors fulfilling the specification.

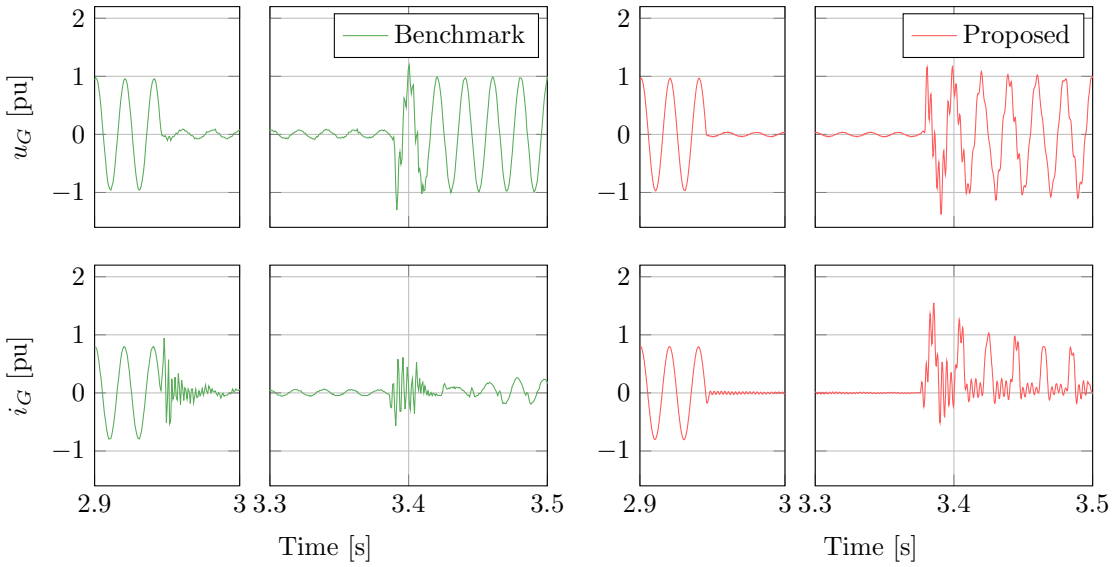

Fig. 10: HIL simulation of grid voltages and currents after a fault in the utility grid.

Power Reference Step and Load Step

As a further test, a power reference step is applied to the converter and the active power trajectory $P_{\text{G,filt}}$ is monitored and shown in Fig. 11. The trajectories of benchmark and proposed design are comparable and are complying with the design requirements, both in terms of time response and reference tracking.

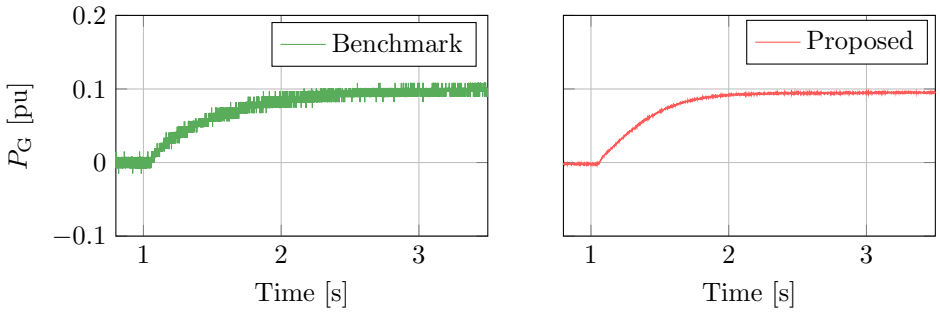

Fig. 11: HIL simulation of active power trajectory after a power reference step.

The reaction of the converter to a load step from 0 p.u. to 0.5 p.u. as shown in Fig. 12 is similarly compliant and comparable.

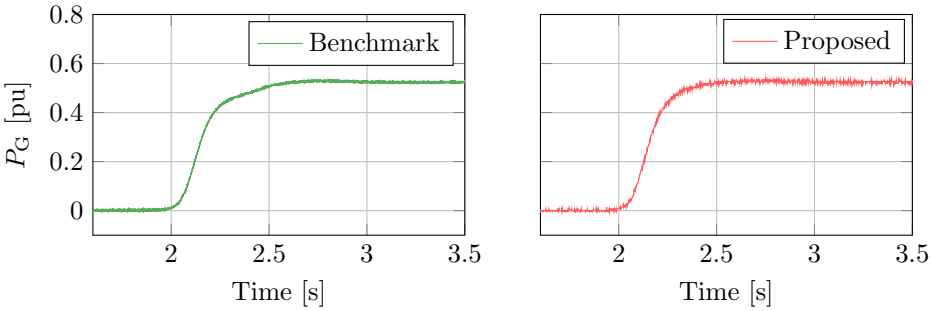

Fig. 12: HIL simulations of active power trajectory after a load step.

Conclusion

This paper suggests a multi-objective optimization procedure for power converters. The procedure has been derived and tested on an MMC topology. The suggested multi-objective optimization method enables an automated system design and aims to optimize an entire converter system for a set of objectives and constraints instead of an individual optimization of components. An analysis of the design space has been demonstrated, evaluating various design parameters and assessing their impact. This reduces the design space and allows a targeted optimization. The pareto-optimal system designs can be compared and assessed by the designer. Thus, the performance can be maintained with a reduced number and size of components, which leads to an improvement of the system in terms of cost or losses. The concept has been verified by offline computer and real-time simulations of steady-state and transient behavior of derived designs, which confirm the benefits of a derived candidate. As future work, the integration of dynamic behavior in the automated optimization would complement the optimization.

References

[1] A. Lesnicar, R. Marquardt: A new modular voltage source inverter topology, In Conf. Rec. EPE, 2003.
[2] S. Debnath, J. Qin, B. Bahrani, M. Saeedifard and P. Barbosa: Operation, Control, and Applications of the Modular Multilevel Converter: A Review, in IEEE Transactions on Power Electronics, vol. 30, no. 1, pp. 37-53, 2015.
[3] T. Thurnherr, P. Maibach, B. Buchmann and E. Baerlocher: Static Frequency Converters for Railway Power Supply based on IGCT High Power Semiconductors, PCIM Europe digital days 2020; International Exhibition and Conference for Power Electronics, Intelligent Motion, Renewable Energy and Energy Management, 2020, pp. 1-8.
[4] D. Weiss, M. Vasiladiotis, C. Banceanu, N. Drack, B. Odegard and A. Grondona: IGCT based Modular Multilevel Converter for an AC-AC Rail Power Supply, PCIM Europe 2017; International Exhibition and Conference for Power Electronics, Intelligent Motion, Renewable Energy and Energy Management, 2017, pp. 1-8.
[5] A. Hillers and J. Biela: Optimal design of the modular multilevel converter for an energy storage system based on split batteries, 15th European Conference on Power Electronics and Applications, 2013, pp. 1-11.
[6] S. Fuchs, M. Jeong and J. Biela: Reducing the Energy Storage Requirements of Modular Multilevel Converters with Optimal Capacitor Voltage Trajectory Shaping, 22nd European Conference on Power Electronics and Applications, 2020, pp. P.1-P.11.
[7] R. Sahu and S. Sudhoff: Design Paradigm for Modular Multilevel Converter-Based Generator Rectifier Systems, in IEEE Open Access Journal of Power and Energy, vol. 7, pp. 130-140, 2020.
[8] S. Am, P. Lefranc, D. Frey and M. Ibrahim: A generic virtual prototyping tool for multilevel modular converters (MMCs), IECON 2015 - 41st Annual Conference of the IEEE Industrial Electronics Society, 2015, pp. 1489-1494.
[9] G. Chiandussi, M. Codegone, S. Ferrero, F.E. Varesio: Comparison of multi-objective optimization methodologies for engineering applications, Computers and Mathematics with Applications, vol. 63, Issue 5, 2012, pp. 912-942.
[10] Luis Martí, Jesús García, Antonio Berlanga, José M. Molina: A stopping criterion for multi-objective optimization evolutionary algorithms, Information Sciences, vol. 367–368, 2016, pp. 700-718.